High Precision Active Nutation Control of a Momentum Biased Spacecraft with Flexible Appendages

R.A. Laskin* and E. H. Kopf†
Jet Propulsion Laboratory, California Institute of Technology, Pasadena, California

The controller design for the Solar Dynamics Observatory, a momentum biased spacecraft with three flexible appendages, is presented. The pointing of scientific instruments imposes arc-second pointing requirements on the spacecraft bus and meeting these requirements necessitates the use of an active nutation controller, here mechanized with a small reaction wheel oriented along a bus transverse axis. The active nutation controller does its job by orchestrating the transfer of angular momentum out of the bus transverse axes and into the momentum wheel. A simulation study verifies that the controller provides quick, stable, and accurate response.

Nomenclature

C = MAG boom torsional damping constant
h = MAG boom attachment point
h_x = negative x RAP boom attachment point
h_z = negative z RAP boom attachment point
I_a = moment of inertia in x of the MAG boom about its own center of mass
I_b $\triangleq m_b \ell\ (x_b + \ell)$
I_h $\triangleq m_b \ell^2$
I_N = spin axis moment of inertia of nutation controller wheel
I_r = spin axis moment of inertia of momentum wheel rotor
I_T $\triangleq \sqrt{I_{yy} I_{zz}}$
I_x^i $\triangleq m_x^i \ell_x^i (x_x + \ell_x^i)$
I_z^i $\triangleq m_z^i \ell_z^i (x_z + \ell_z^i)$
I_{xx}, I_{yy}, I_{zz} = spacecraft x, y, z moments of inertia
I_{xx}^i $\triangleq m_x^i (\ell_x^i)^2$
I_{zz}^i $\triangleq m_z^i (\ell_z^i)^2$
K = MAG boom torsional spring constant
ℓ = length of MAG boom lollipop
ℓ_x^i = length of ith negative x boom lollipop
ℓ_z^i = length of ith negative z boom lollipop
m_b = lumped mass of the MAG boom
m_x^i = lumped mass of the ith lollipop in the negative x RAP boom
m_z^i = lumped mass of the ith lollipop in the negative z RAP boom
n_x, n_y, n_z = unit vector along spacecraft bus axes x, y, z, respectively
Q = MAG boom bending damping constant
Q_i = bending damping constant for ith lollipop in RAP boom (negative x and negative z booms)
R = MAG boom bending spring constant
R_i = bending spring constant for ith lollipop in RAP boom (negative x and negative z booms)
x, y, z = spacecraft central principle axes (pitch, yaw, roll, respectively)
x_b, x_x, x_z = distance from spacecraft c.o.m. to points h, h_x, h_z, respectively
α = angle of momentum wheel rotor with respect to the spacecraft bus
β = bending angle of MAG boom lollipop about y
γ = bending angle of MAG boom lollipop about z
δ = torsional angle of MAG boom lollipop about x
ϵ_i = bending angle of ith lollipop in negative x RAP boom about y
ζ = alignment error angle of the rotor spin axis (error about z axis only)
η = angle of the active nutation controller wheel with respect to the spacecraft bus
η_i = bending angle of ith lollipop in negative x RAP boom about z
λ_i = bending angle of ith lollipop in negative z RAP boom about x
μ_i = bending angle of ith lollipop in negative z RAP boom about y
ϕ, θ, ψ = pitch, yaw, roll (1-2-3) Euler angles
ω = spacecraft bus inertial angular velocity
ω_x = $n_x \cdot \omega$
ω_y = $n_y \cdot \omega$
ω_z = $n_z \cdot \omega$

Presented as Paper 83-330 at the AAS/AIAA Astrodynamics Specialist Conference, Lake Placid, N.Y., Aug. 22-25, 1983; received Oct. 24, 1983; revision received March 28, 1984.

*Member Technical Staff, Guidance and Control Section. Member AIAA.
†Member Technical Staff, Guidance and Control Section.

Introduction

THE Solar Dynamics Observatory (SDO) in its current configuration is a flexible momentum biased spacecraft with two active control loops that provide three-axis stabilization. The primary scientific instrument, a solar oscillations imager (SOI), is rigidly mounted to the spacecraft bus and must be pointed with very high precision (± 10 arc-sec absolute error, ± 4 arc-sec stability over any 200-s interval) at the sun. Usually, momentum biased spacecraft are controlled via a single control loop that acts by applying torques to the momentum wheel. This loop provides bus attitude regulation about the momentum wheel axis only. Control about the other two axes (viz. the transverse axes) is accomplished passively by utilizing a nutation damper. The design and performance of such devices is well documented in the literature. The problem for SDO lies in the fact that the tight pointing requirements mandate an operating regime that would put most passive dampers below their mechanical thresholds. Even those that could successfully dissipate energy in the arc-second pointing regime would not do so at a rate sufficiently high to be effective. Hence, a scheme for active nutation control is called for.

The literature contains three basic approaches to the active nutation control problem: use of mass properties (i.e., cross products of inertia) to facilitate nutation control via momentum wheel torquing,[1-3] the use of a control moment

gyro (CMG),[4] and the use of a small reaction wheel whose spin axis is aligned along one of the bus transverse axes.[5] We have chosen the third approach, but with a modified control law. The salient new feature is a controller transfer function tuned to the nutation frequency. This approach tends to maximize the rate of angular momentum transfer out of the bus transverse axes and into the momentum wheel. It is seen that the two controllers must work in concert to accomplish this momentum transfer.

An added complication arises for SDO due to the presence of three flexible booms: two radio astronomy and plasma wave experiment (RAP) booms and one magnetometer (MAG) boom. The two RAP booms are sufficiently flexible ($\sim$0.125 Hz) so that their natural frequencies cannot be kept out of the contoller bandwidth. The controllers are designed on the basis of linearized equations for a nonflexible spacecraft. They are then tested on the full nonlinear equations, including flexibility, via a digital simulation. The simulation results show that while flexibility *does* degrade controller performance, it can neither drive the system unstable nor threaten SDO mission requirements.

Spacecraft Dynamics

A schematic representation of the spacecraft mathematical model is shown in Fig. 1. Notice that the booms have each been represented by lumped mass models. Each RAP boom, one along negative x, the other along negative z, appears as a rigid "lollipop" with all its mass concentrated at a point at the end of a massless link. Flexibility has been confined to the point of attachment with the spacecraft bus, where it takes the form of a spring that resists boom "bending" in any direction. RAP boom torsional motion has been ignored here, since it was found that the lowest RAP torsional frequency ($\sim$60 Hz) is sufficiently high to preclude significant interaction with either of the two active control loops. The MAG boom is modeled in the same way, except that its torsional motion *is* taken into account. This is done by regarding the boom as a point mass in the y-z directions and as having nonzero moment of inertia about its center of mass only in x. Torsional motions of the MAG boom are resisted by a torsional spring located coincidentally with the bending spring at the boom's base. Notice in Fig. 1 that all symbols pertaining to the RAP booms are either subscripted or superscripted with the letter i. This is to indicate that each of these booms may be represented not by a single "lollipop," but by a *set* of lollipops aimed at representing a set of significant RAP boom bending modes. Although in the simulation study presented later attention is confined to the fundamental RAP mode, the capability of modeling multiple modes is retained here for the sake of generality. The method used for representing flexible appendages as sets of lumped mass models is due to Ref. 6.

Three important assumptions/approximations underlie the dynamical analysis: 1) All boom motions are restricted to small angles. 2) The axes x, y, z are fixed in the spacecraft bus. They are the central principle axes for the spacecraft and remain so even when the booms are not in their equilibrium positions. 3) The spacecraft experiences no translational accelerations.

To begin, there are $4+2n$ bodies in the model of Fig. 1, n being the number of lollipops comprising each RAP boom. (See Nomenclature.) These bodies are denoted as follows:

D = spacecraft bus
R = momentum wheel rotor
N = nutation controller wheel
B = RAP boom lollipop
B_i^x = ith lollipop in negative x RAP boom
B_i^z = ith lollipop in negative z RAP boom

There are $8+4n$ degrees of freedom embodied by the coordinates ω_x, ω_y, ω_z, α, η, β, γ, δ, ϵ_i, η_i, λ_i, and μ_i. The approach to deriving the $8+4n$ equations of motion is to apply the angular momentum principle, $T=\dot{H}$, repeatedly; first to the spacecraft as a whole, and then to bodies R, N, B, B_i^x, B_i^z in turn.

The only subtlety involved is in choosing the attach point of each boom as that boom's reference point for application of the angular momentum principle. Since these points are neither mass centers of their respective booms, nor are they inertially fixed, the momentum principle $T=\dot{H}$, must be augmented with a "correction" term in order to remain valid. The derivation of dynamical equations is otherwise straightforward. The full nonlinear equations that result are presented in Ref. 7. Presented here are equations that have been linearized about a nominal motion of quiescent pointing (i.e., $\omega_x \equiv \omega_y \equiv \omega_z \equiv \eta \equiv \delta \equiv \beta \equiv \gamma \equiv \epsilon_i \equiv \eta_i \equiv \lambda_i \equiv \mu_i \equiv 0$: $\dot{\alpha}(t) =$ const);

$$I_{xx}\dot{\omega}_x + I_r\ddot{\alpha} = T_x - I_N\dot{\eta}\omega_y \tag{1}$$

$$I_{yy}\dot{\omega}_y + I_b\ddot{\beta} = T_y - I_r\dot{\alpha}\omega_z + I_N\dot{\eta}\omega_x \tag{2}$$

$$I_{zz}\dot{\omega}_z + I_N\ddot{\eta} + I_b\ddot{\gamma} = T_z + I_r\dot{\alpha}\omega_y \tag{3}$$

$$I_r(\ddot{\alpha} + \dot{\omega}_x) = T_r \tag{4}$$

$$I_N(\ddot{\eta} + \dot{\omega}_z) = T_N \tag{5}$$

$$I_h\ddot{\beta} + I_b\dot{\omega}_y = -Q\dot{\beta} - R\beta \tag{6}$$

$$I_h\ddot{\gamma} + I_b\dot{\omega}_z = -Q\dot{\gamma} - R\gamma \tag{7}$$

$$I_a(\ddot{\delta} + \dot{\omega}_x) = -C\dot{\delta} - K\delta \tag{8}$$

$$I^i_{xx}\ddot{\epsilon}_i + I^i_x\dot{\omega}_y = -Q_i\dot{\epsilon}_i - R_i\epsilon_i \tag{9}$$

$$I^i_{xx}\ddot{\eta}_i + I^i_x\dot{\omega}_z = -Q_i\dot{\eta}_i - R_i\eta_i \tag{10}$$

$$I^i_{zz}\ddot{\lambda}_i + I^i_z\dot{\omega}_x = -Q_i\dot{\lambda}_i - R_i\lambda_i \tag{11}$$

$$I^i_{zz}\ddot{\mu}_i + I^i_z\dot{\omega}_y = -Q_i\dot{\mu}_i - R_i\mu_i \tag{12}$$

The only coordinates not considered to be small in the linearization process are α and η. Note that rotor mis-

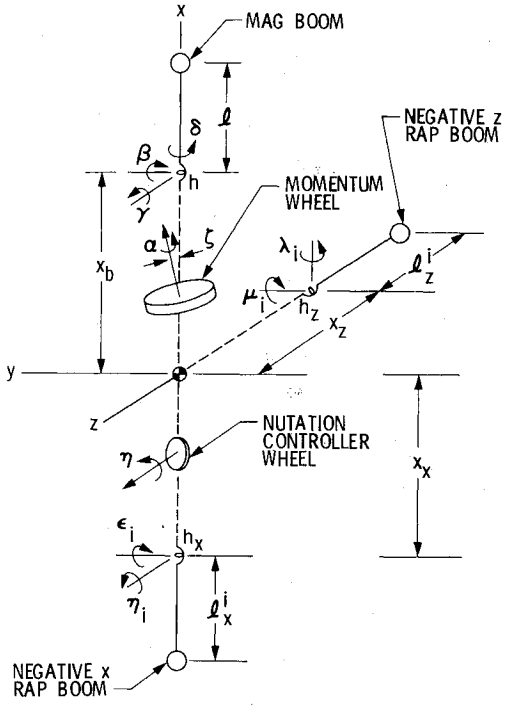

Fig. 1 Solar dynamics observatory schematic.

alignment has been ignored above (i.e., $\zeta=0$). From a dynamical point of view these equations are inherently stable. Results governing the stability of dual-spin spacecraft (which SDO formally is) identify the magnitude and location(s) of energy dissipation as the critical factors in determining stability.[8] For the case at hand, energy dissipation on the spacecraft bus is always stabilizing, while dissipation on the rotor has the opposite effect. But the idealized system of Fig. 1 allows energy dissipation only on the bus at the boom hinge points, and thus the booms effectively act as "untuned" nutation dampers, providing system stability regardless of the spacecraft inertia ratio I_{xx}/I_T. Of course, the actual spacecraft will contain other sources of energy dissipation (not the least of which is a passive, *tuned* nutation damper) and two active control loops as well. These will significantly increase the complexity of the stability question. Yet the importance of the fact that the spacecraft model is dynamically stable should not be underestimated. It gives credence to the intuitive notion that the two low-authority controllers will have a difficult time introducing any instability. The results of the simulation study strongly confirm this observation.

Spacecraft Control

Figure 2 depicts the overall control design concept for SDO. The objective is precision pointing (± 10 arc-sec absolute, ± 4 arc-sec stability for 200 s) of the SOI (solar oscillations imager), which is oriented along the z axis, at the sun. This can be regarded as consisting of three tasks:

1) Correct for yaw axis (y) drift of the angular momentum vector, $\boldsymbol{H}$, from its nominal inertial orientation perpendicular to the ecliptic plane.

2) Reduce coning behavior, $\theta_N \to 0$, thus tending to align the pitch axis (x) with the $\boldsymbol{H}$ vector.

3) Drive the pointing error about the pitch axis to zero.

The first of these is handled by microprecession thrusters (located at stations 1, 2, 3, and 4 in Fig. 2) which provide precision yaw axis drift control with 0.2 arc-sec step capability via torque impulses about the roll axis. An ideal thruster pulse will instantaneously reorient the $\boldsymbol{H}$ vector and precipitate spacecraft coning at a cone angle θ_N that depends on the strength of the pulse.

Removing this coning motion and any pitch error that may accompany it is the job of the two active control loops, the active nutation controller (ANC) and the pitch axis controller (PAC). The former operates by managing the momentum in the little reaction wheel aligned with the roll axis (z); the latter operates through momentum wheel torquing. Both controllers were initially designed in Ref. 9. The approach was to ignore the complications posed by boom flexibility and nonlinearity of the dynamical equations as well as coupling between the two controllers via spacecraft dynamics. The straightforward, linear controllers that result have been tested on the full-scale simulation model and shown to be impressively robust.

The pitch axis can be adequately controlled in a variety of ways. Our approach is described briefly below. Attention, however, is focussed on the active nutation controller. We first formally present the details of the ANC design which incorporates a "tuned" filter along with positive feedback. There follows a discussion of the physical mechanism that underlies the ANC's effectiveness. It is seen that the active nutation controller and the pitch axis controller work together to orchestrate the transfer of angular momentum out of yaw/roll and into the momentum wheel rotor.

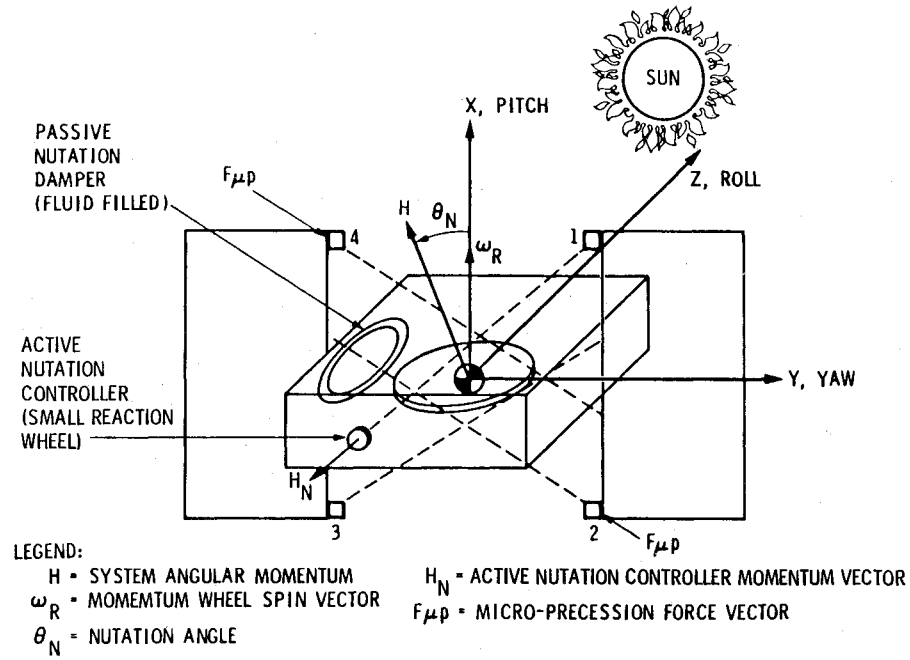

Fig. 2 Spacecraft control concept.

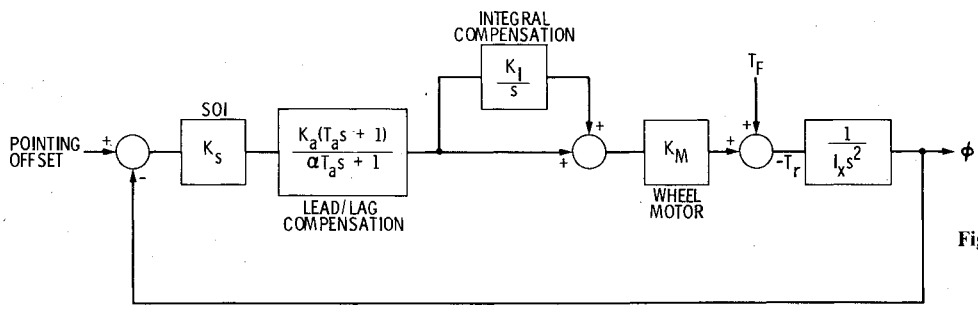

Fig. 3 Pitch axis controller block diagram.

Pitch Axis Controller

Figure 3 is a block diagram of the lead/lag compensated proportional plus integral controller that handles pitch axis bus pointing control via momentum wheel torquing. Since flexibility effects, nonlinearities in the dynamical equations, and interaction with the ANC all have been ignored, the relevant pitch axis equations of motion are simply

$$I_{xx}\dot{\omega}_x + I_r\ddot{\alpha} = 0 \tag{13}$$

$$I_r(\ddot{\alpha} + \dot{\omega}_x) = T_r \tag{14}$$

$$\dot{\phi} = \omega_x \tag{15}$$

These readily combine to give the plant equation as

$$I_x\ddot{\phi} = -T_r(t) \tag{16}$$

where $I_x = I_{xx} - I_r$. As the block diagram illustrates, the pitch axis torque on the spacecraft bus (i.e., $-T_r$) will consist of two parts: the wheel motor control torque and the wheel bearing Coulomb friction torque T_F. The latter represents about 33% of the maximum motor torque and hence would lead to a sizeable ($\sim$7 arc-sec) steady-state pointing error were it not for the presence of the integral compensation. Of course one pays a price for introducing integral action since it is invariably accompanied by a reduced stability margin. This is reflected in Fig. 4 which is a rough root locus plot for the controller of Fig. 3. Notice that at sufficiently low forward gain the system is unstable. A careful choice of the gains as well as the other pitch controller parameters provides a stable system with a phase margin of 42 deg and a bandwidth of about 1 Hz. Values for the controller parameters are listed in Table 1.

It should be emphasized that although the above remarks describe a pitch controller that is linear, the simulation program in fact incorporates three realistic nonlinear features in the controller "implementation": 1) the SOI sensor, lead/lag network, integrator, and wheel motor all saturate at realistic levels, 2) sensor resolution is accounted for, and 3) motor hysteresis is included.

As will be seen later, controller saturation presents no problem when the spacecraft is operating in the arc-sec, quiescent pointing regime. The effect of motor hysteresis is to introduce a very small bus angle limit cycle ($\sim$0.3 arc-sec for 5% hysteresis). Sensor resultuion, at least at the level anticipated for the SOI internal sun sensor, leaves controller performance virtually unaffected.

Active Nutation Controller

The active nutation controller (ANC) is a more involved system than the pitch controller just considered. The relevant linearized equations of motion are

$$I_{yy}\dot{\omega}_y + I_r\dot{\alpha}\omega_z = 0 \tag{17}$$

$$I_{zz}\dot{\omega}_z - I_r\dot{\alpha}\omega_y = -I_N\ddot{\eta} \tag{18}$$

$$I_N(\ddot{\eta} + \dot{\omega}_z) = T_N \tag{19}$$

$$\dot{\theta} = \omega_y \tag{20}$$

where flexibility effects are neglected and the pitch controller is assumed ideal so that $\phi \equiv \omega_x \equiv 0$. In bare outline, the controller design is as follows: The SOI sensed yaw axis error angle, $\theta(t)$, is fed through a second order filter "tuned" to the precession frequency; the filtered signal, nominally 90 deg out of phase with $\theta(t)$, is amplified and used to drive a simple speed control loop that is placed around the nutation wheel motor; the output, $\dot{\eta}(t)$, is a wheel speed modulated to act in synchronism with the bus precession frequency. The result, as documented in the simulation study, is a highly effective controller whose method of action can be explained in terms of angular momentum transfer out of the transverse body axes and into the momentum wheel rotor.

A block diagram for the ANC appears in Fig. 5. The "plant" block in the figure is derived by eliminating ω_y and ω_z from Eqs. (17), (18), and (20) and arriving at:

$$\ddot{\theta} + \omega_0^2\theta = \frac{I_N}{I_T}\omega_0\dot{\eta} \tag{21}$$

where $\omega_0 = I_r\dot{\alpha}/I_T$ is the precession frequency. The most startling feature of Fig. 5 is the presence of positive feedback. Perhaps the loop can be best understood by regarding the feedback as negative and taking the forward gain to be negative as well. Then the negative gain root locus plot can be drawn as in Fig. 6 where, for the sake of simplicity, the pole associated with the speed control loop has been moved out to negative infinity (ideal speed response). The root locus reveals that the system is low gain stable, high gain unstable. The controller parameters are given in Table 2.

As with the pitch controller, the simulation program incorporates certain nonlinearities into the ANC implementation. Foremost among these are various saturation limits around the loop and Coulomb friction in the ANC wheel bearing.

Mechanism of ANC Momentum Transfer

Since the design of the active nutation controller is rather unconventional, it is worthwhile to trace the physical basis for its effectiveness. Consider the steady precessional behavior pictured in Figs. 7 and 8. Assuming an effective pitch axis controller ($\phi \approx \omega_x \approx 0$) and a relatively low-authority ANC, the actual coning behavior cannot look too different from that shown in the figures. Taking the instant captured in Fig.

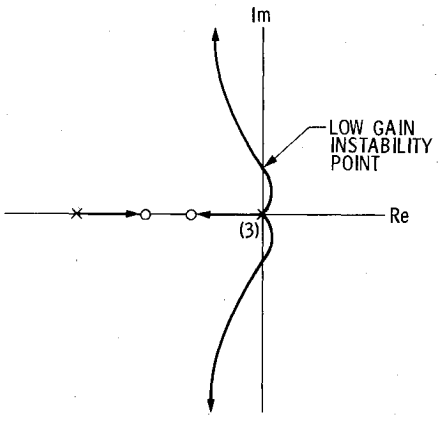

Fig. 4 Pitch axis controller root locus plot.

Table 1 Pitch axis controller parameter values

$K_s = 50{,}000$ V/rad	$K_I = 1.0\ \text{s}^{-1}$
$K_a = 5.8$ V/V	$K_M = 0.0025$ N-m/V
$T_0 = 2.0$ s	$T_F = 0.025$ N-m
$\alpha = 0.067$	

Table 2 Active nutation controller parameters

$K_s = 50{,}000$ V/rad	$K_a = 30$ V/V
$\zeta = 0.8$	$K_m = 0.00125$ N-m/V
$K_{ND} = 2.8$ (rad/s)/V	$K_T = 0.0764$ V/(rad/s)
$I_N = 3 \times 10^{-4}$ kg-m^2	

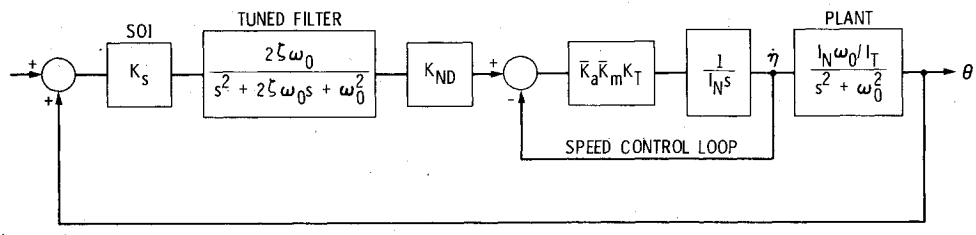

Fig. 5 Active nutation controller block diagram.

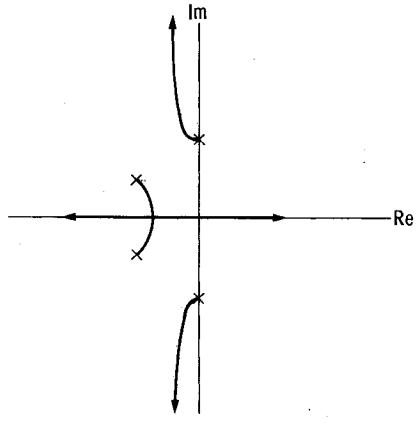

Fig. 6 Active nutation controller root locus plot.

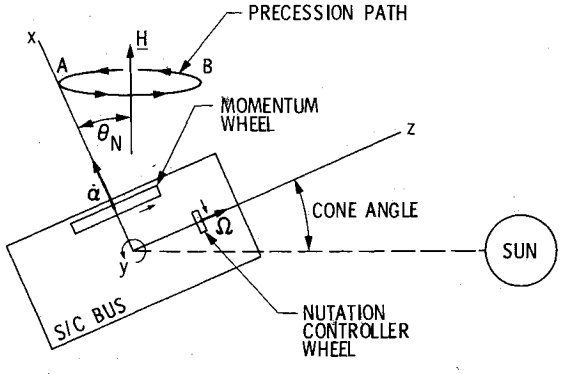

Fig. 7 Spacecraft undergoing steady precession.

7, where $\boldsymbol{H}$ lies in the x-z plane, to be time zero, we have:

$$\omega_y(t) = \frac{-\bar{\theta}_N}{\omega_0} \sin\omega_0 t \tag{22}$$

$$\omega_z(t) = \frac{I_T \bar{\theta}_N}{I_{zz}\omega_0} \cos\omega_0 t \tag{23}$$

$$\theta(t) = \bar{\theta}_N \cos\omega_0 t \tag{24}$$

where $\bar{\theta}_N = \theta_N(0) = \theta(0)$. After the motion progresses through half a precession period, the system will appear as illustrated in Fig. 8 with $\boldsymbol{H}$ again lying in the x-z plane. The net effect is a negative rotation about the y axis through the angle $2\bar{\theta}_N$. Although the x axis describes a curvilinear (coning) path during the course of this motion, the z axis remains in the same plane throughout (i.e., the plane established by the $\boldsymbol{H}$ vector and the sun). Thus the ANC wheel is constrained to perform a planar rotation through the angle $2\bar{\theta}_N$ and at the angular rate $\omega_y(t)$.

It is now supposed that during the duration of this planar rotation the wheel is forced to maintain the constant spin Ωn_z shown in Fig. 7. Such a precessional motion requires an

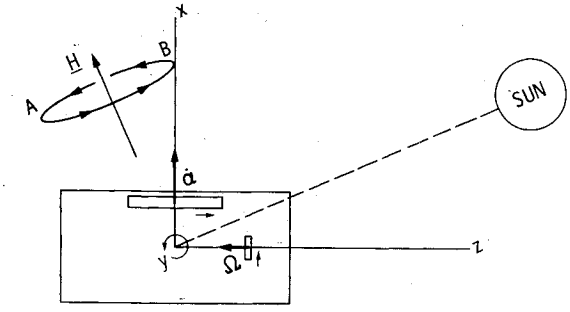

Fig. 8 Nutation wheel spin reversal.

applied torque whose component in the x direction is given by

$$T_x = I_N \Omega \omega_y \tag{25}$$

This torque, which will be negative due to the sign of $\omega_y(t)$, must be supplied by the spacecraft bus at the ANC wheel bearings. Of course, the bus itself experiences an equal and opposite torque, one tending to induce a bus rotation about the positive x axis. However, the pitch servo will act to counter this incipient bus rotation and in so doing will torque the momentum wheel in a positive sense, increasing its angular rate. Thus the ANC, by maintaining a constant wheel spin while the spacecraft precesses from point A to point B (see Figs. 7 and 8), will pump momentum into the momentum wheel through the agency of the pitch controller. And if at point B the ANC's wheel spin is instantaneously reversed (Fig. 8), this process of momentum transfer out of the transverse axes and into the momentum wheel will continue unabated. It should be noted that due to hardware considerations the wheel spin reversal actually will be implemented by two counter-rotating wheels, each operating unidirectionally. And, of course, wheel speeds will not be changed instantaneously, but rather in the smooth sinusoidal fashion dictated by the controller of the previous section. However, the qualitative thrust of the argument does not change and so long as the ANC wheel is driven out of phase with $\omega_y(t)$, insuring that T_x in Eq. (25) is negative, momentum will flow in the proper direction.

The above idealized analysis involving instantaneous changes in wheel speed can be carried a step further to provide an upper bound on the expected rate of nutation angle subsidence. Since θ_N is a small angle, we have the following relationships

$$\Delta\theta_N = \Delta H_z / H_x \tag{26}$$

$$\Delta H_z / H_x = -\Delta H_x / H_z(0) \tag{27}$$

where Δ specifies the change in a particular quantity over half a precession period (e.g., from point A to point B of the figure). In addition we have

$$H_z(0) = I_{zz}\omega_z(0) = I_T \bar{\theta}_N / \omega_0 \tag{28}$$

$$\Delta H_x = -\int_0^{\pi/\omega_0} T_x dt = \frac{I_N \Omega \bar{\theta}_N}{\omega_0} \int_0^{\pi/\omega_0} \sin\omega_0 t dt = \frac{2\bar{\theta}_N I_N \Omega}{\omega_0^2} \quad (29)$$

Combining Eqs. (26-29) provides

$$\Delta\theta_N = -2I_N\Omega/I_T\omega_0 \quad (30)$$

Dividing this angular change by half the precession period, π/ω_0, gives an approximate value for the best case rate of change of the nutation angle:

$$\dot{\theta}_N = -2I_N\Omega/\pi I_T \quad (31)$$

Current parameter values establish this number at 7 arc-sec/s which is confirmed by simulation results as a good upper bound.

To retrace the flow of angular momentum: transverse bus momentum is dumped into the ANC wheel and thence, with the help of the pitch controller, is transferred into the momentum wheel. As the transverse momentum decreases, the pitch axis approaches alignment with the $\boldsymbol{H}$ vector and quiescent pointing is established.

Simulation Study

A computer program was developed to simulate spacecraft dynamics and control. This program has been used to conduct a simulation study aimed at validating the controller design and at determining the flexible body design constraints that must be satisfied by the two RAP booms.

Before the simulation results are presented, let us first define the pointing error variables, CLOCK and CONE. The pointing error angle is simply the angle between the spacecraft bus z axis (along which the SOI is oriented) and the spacecraft-sun line. CLOCK is the projection of this angle onto the ecliptic plane. CONE is the projection of this angle onto the plane containing the spacecraft-sun line and perpendicular to the ecliptic plane. For the purposes of this study, where the bus attitude angles are always small, CLOCK is virtually identical to the pitch angle ϕ and CONE is simply the yaw angle θ.

Spacecraft Behavior Without Flexibility

In order to assess the degradation in pointing performance caused by the three flexible booms, it is necessary first to consider the idealized case of the three rigid body system consisting of the spacecraft bus, the momentum wheel rotor, and the ANC wheel. This also affords a good opportunity to check out the nominal functioning of the two controllers.

The major source of controller activity for the quiescent pointing mode is expected to be yaw axis drift due to very small roll disturbance torques. The control strategy will be to let the bus drift accumulate until some CONE angle is attained, then reorient the $\boldsymbol{H}$ vector with a microprecession thruster pulse and let the controllers do their job of attenuating the resulting motion. (Depending on the amount of drift that is allowed to accumulate and the desirability of maintaining science measurements uninterrupted, a multipulse approach may be implemented.) Assume 10 arc-sec of accumulated drift and one ideal torque impulse. Spacecraft response is as depicted in Fig. 9. Note that the nutation dynamics excite only a very weak and short-lived transient in the pitch loop. (This decoupling between the two control loops is reciprocal, i.e., pitch dynamics excite yaw/roll only minimally.) The active nutation controller exhibits a time constant of ~10 s and functions far below its saturation levels. Even when driven into saturation by large CONE errors, the ANC will continue to function effectively since the output of the tuned filter will still be a sinusoid at the nutation frequency and with the proper phase shift. In fact, it is only in saturation that the ANC approaches its theoretical capability of 7 arc-sec/s CONE angle attenuation.

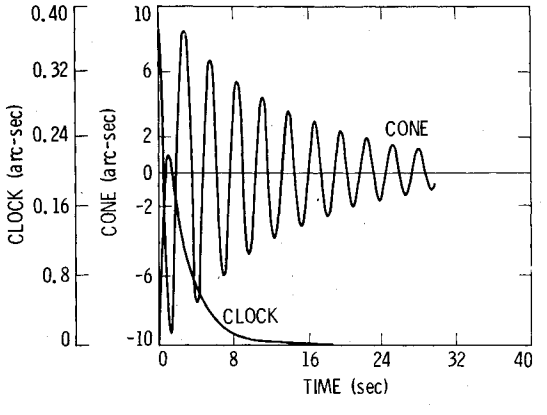

Fig. 9 Pointing error angles—spacecraft without flexibility.

Flex-Body Considerations

The above results make it clear that without the booms, spacecraft performance would be more than adequate. The questions that arise are: What effect do the booms have on spacecraft performance? Will they induce instability or merely degrade performance? If the latter, will the new level of performance be acceptable?

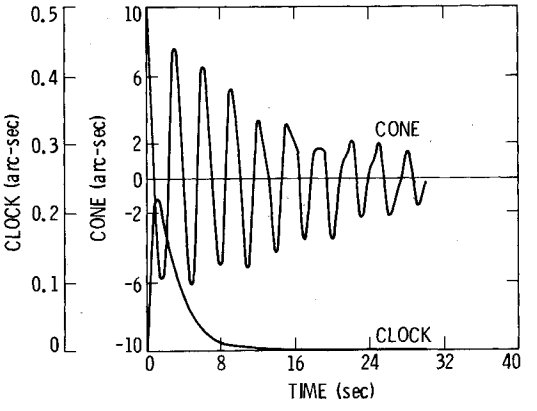

Fig. 10 Pointing error angles—nominal RAP booms.

Table 3 Boom configurations

	MAG boom	RAP boom, nominal case (Voyager booms)
Mass, kg	4.45	0.09662
Length, m	3.0	7.264
Bending frequency, Hz	0.5	0.129
Torsional frequency, Hz	1.0	–
Torsional moment of inertia, kg-m^2	0.0115	–

RAP boom, variations from nominal case

Case	Frequency	Times mass
a	Same	10 times
b	Same	100 times
c	1/4	Same
d	1/4	10 times
e	1/4	100 times
f	4 times	Same
g	4 times	10 times
h	4 times	100 times

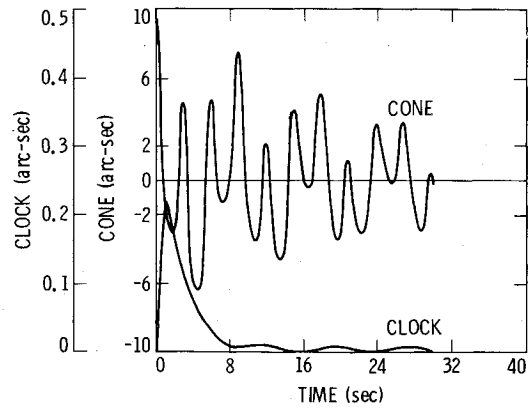

Fig. 11 Pointing error angles—case a RAP booms.

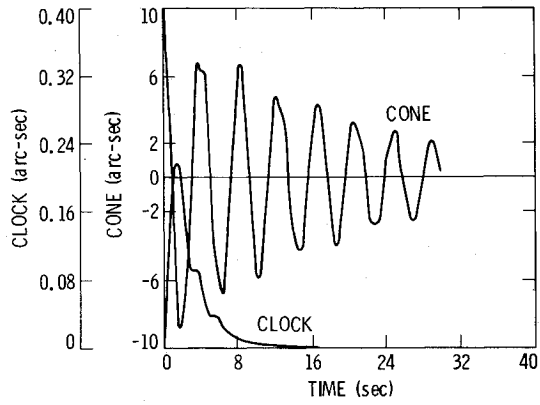

Fig. 12 Pointing error angles—case g RAP booms.

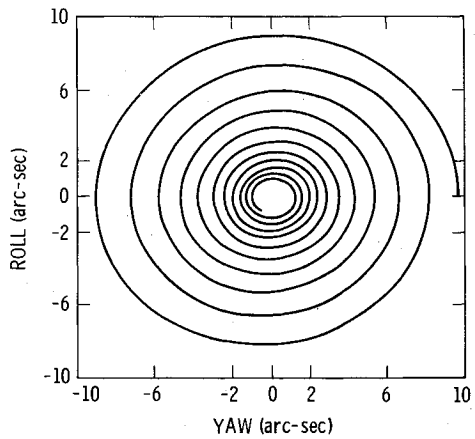

Fig. 13 Yaw/roll phase plane plot—spacecraft without flexibility.

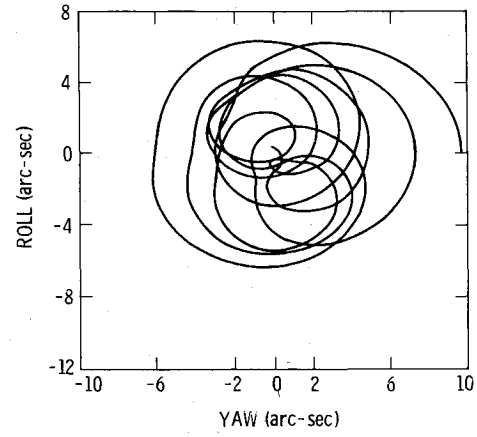

Fig. 14 Yaw/roll phase plane plot—case a RAP booms.

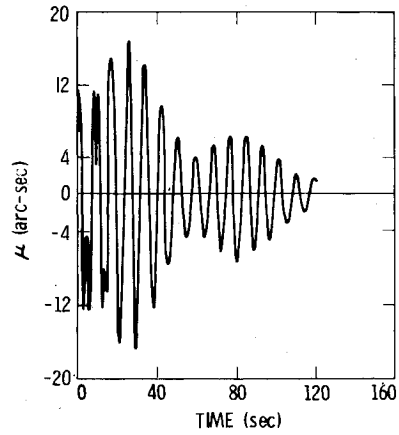

Fig. 15 Negative x RAP boom bending about yaw—case a RAP boom.

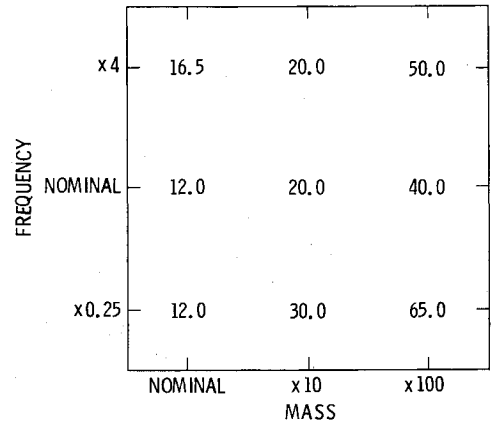

Fig. 16 Nutational time constants (in seconds) for various RAP boom cases.

The approach taken here in addressing these questions is to examine the effect on spacecraft behavior of varying the boom parameters (i.e., stiffness and mass). Running the simulation program for several combinations of boom parameters can give us useful general information and also point to specific boom configurations which should be cautiously regarded. The scenario of interest is that discussed above, a microprecession maneuver to correct for yaw drift. Assume the same 10 arc-sec of accumulated drift and an ideal torque impulse. The boom configurations considered are given in Table 3.

The values given are for the lollipop models used in the simulation. Attention has been focused on the RAP booms because their natural frequencies are expected to be well down in the controller bandwidths ($\sim$1 Hz for the pitch controller and 0.35 Hz for the ANC). The nominal case corresponds to the RAP booms that flew on the two Voyager space. The other RAP boom simulation cases explore the boom parameter space in the vicinity of the nominal case. It should be noted that case g of Table 3 coresponds to an off-the-shelf boom manufactured by Fairchild Corporation. All boom models, MAG boom included, contain 1% "structural damping."

Typical simulation results appear in Figs. 10-12. Comparison with Fig. 9 reveals that flexibility causes a

degradation in pointing performance but does *not* lead to instability. This is also seen in Figs. 13 and 14 which are phase plane plots of the yaw/roll angles (an observer looking down the H vector at the tip of the pitch axis would see these trajectories traced). The booms themselves also exhibit stable response, although bus coning energy can be pumped into certain boom modes on a transient basis (see Fig. 15).

Perhaps the apparent robustness of the controlled system should not occasion any surprise. After all, the spacecraft (including flexibility) is dynamically stable. The pitch axis controller, although of low authority, is seen to be quite quick in the arc-second pointing regime. The time constant for active nutation control (slower than pitch) for the various RAP boom cases is given in Fig. 16. This plot can be used as a measure of system performance and as an indicator of RAP boom specifications that may be unacceptable.

Conclusion

The approach to active nutation control presented above has been shown to be an effective means of achieving quick and stable arc-second pointing for momentum biased and dual-spin spacecraft, even in the presence of flexible appendages whose natural frequencies lie within the controller bandwidth. Future work in this area might concentrate on a comparison of the performance, cost, and limitations of the various schemes for active nutation control that now exist in the literature.

Acknowledgments

The research described in this paper was performed at the Jet Propulsion Laboratory, California Institute of Technology, under contract with the National Aeronautics and Space Administration.

References

[1] Phillips, K.J., "Active Nutation Damping Utilizing Spacecraft Mass Properties," *IEEE Transactions on Aerospace and Electronic Systems,* Vol. AES-9, No. 5, Sept. 1973, pp. 688-693.

[2] Leliakov, I.P. and Barba, P.M., "Damping Spacecraft Nutation by Means of a Despun Antenna," Paper No. AAS73-205, presented at the AAS/AIAA Astrodynamics Conference, Vail, Colo., July 1973.

[3] Smay, J.W. and Slafer, L.I., "Dual-Spin Spacecraft Stabilization Using Nutation Feedback and Inertia Coupling," *Journal of Spacecraft and Rockets,* Vol. 13, Nov. 1976, pp. 650-659.

[4] Mingori, D.L., Harrison, J.A., and Tseng, G.T., "Semipassive and Active Nutation Dampers for Dual-Spin Spacecraft," *Journal of Spacecraft and Rockets,* Vol. 8, May 1971, pp. 448-455.

[5] Terasaki, R.M., "Dual Reaction Wheel Control of Spacecraft Pointing," *Proceedings of the Symposium on Attitude Stabilization and Control of Dual-Spin Spacecraft,* Air Force Systems Command and Aerospace Corporation, Aug. 1967, pp. 185-196.

[6] Bamford, R.M., Wada, B.K., and Grayman, W.H., "Equivalent Spring-Mass System for Normal Modes," Jet Propulsion Laboratory Technical Memorandum 33-380, Feb. 1971.

[7] Laskin, R.A. and Kopf, E.H., "High Precision Active Nutation Control for a Flexible Momentum Biased Spacecraft," Proceedings of the AAS/AIAA Astrodynamics Conference, *Advances in the Astronautical Sciences,* Lake Placid, N.Y., Aug. 1983.

[8] Mingori, D.L., "Effects of Energy Dissipation on the Attitude Stability of Dual-Spin Satellites," *AIAA Journal,* Vol. 7, Jan. 1969, pp. 20-27.

[9] Kopf, E.H., "SIS Attitude Control Comments," Jet Propulsion Laboratory Engineering Memorandum 343-724, internal document, June 1982.